




PAPER

[View Article Online](#)
[View Journal](#) | [View Issue](#)


Cite this: *Green Chem.*, 2023, **25**, 5113

A direct pathway for the coupling of arenes and alkylamines *via* a heterogeneous zeolite-based photocatalyst†

Vincent Lemmens,^a Kwinten Janssens, ^a Jorge Gascon ^b and Dirk E. De Vos ^{*a}

The production of *N,N*-dialkyl arylamines is relevant for a range of high-value materials such as pharmaceuticals, agrochemicals and organic materials. In general, these molecules are assembled *via* multiple pre-functionalization steps of the aromatic compound and a subsequent cross-coupling with the arylamine under harsh conditions. In this manuscript, we develop a more sustainable and efficient method for the direct C–H amination of arenes and alkylamines using Ru(bipy)₃²⁺ entrapped in the supercages of a faujasite support (CBV-100). This creates a heterogeneous photocatalyst that can be used under visible light irradiation. Furthermore, the mesomeric and/or inductive effects of the substituent groups on the arene coupling partner are thoroughly investigated using Hammett plots, leading to a rationally guided solvent selection (HFIP or CH₃CN). Using reduced reaction temperatures (<0 °C) drastically improves the product yield, while suppressing the generation of side products.

Received 14th April 2023,
Accepted 7th June 2023

DOI: 10.1039/d3gc01225e

rsc.li/greenchem

Introduction

The construction of carbon–nitrogen bonds is seen worldwide as an extremely important reaction for the manufacture of high value-compounds, such as bulk chemicals, polymers, organic materials, agrochemicals and pharmaceuticals.^{1–4} Moreover, the formation of (di)alkyl arylamines represents about 20–30% of all nitrogen compound manipulations in the current pharmaceutical industry and is therefore of utmost importance in global drug discovery programs.^{1,5,6}

Traditionally, the introduction of nitrogen functional groups on arene substrates is performed by multi-step syntheses, starting from nitration, followed by reduction and additional manipulation steps (Fig. 1).¹ Unfortunately, nitration and subsequent manipulation steps are typically

associated with harsh conditions (*e.g.* strongly acidic, high temperature/pressure) and low selectivity.¹ Interest in the development of other approaches has therefore grown significantly. At the beginning of the twentieth century, Ullmann^{7,8} and Goldberg⁹ (Fig. 1) published their pioneering work on C–N coupling using stoichiometric or even catalytic amounts of copper at elevated temperatures (>200 °C).^{4,10–13} In this context, the Cu-catalyzed Chan–Lam^{14–16} and Pd-catalyzed Buchwald–Hartwig coupling^{17,18} (Fig. 1) were well adopted as new methodologies in industry and academia.¹³ Despite their versatility, all these approaches need pre-functionalized arenes (*e.g.* aryl-boron compounds or aryl halides), which requires additional functionalization steps. Hence, this approach is less suitable for late-stage applications.^{1,2}

More recently, research has shifted towards greener C–H activation strategies, aiming at using unfunctionalized arenes.³ Generally, two different strategies are considered: (1) cross-dehydrogenative C–N couplings (CDC) and (2) electrophilic amination (EA).^{3,19} In the latter approach, the nitrogen coupling partner carries a leaving group on the nitrogen atom, which makes the nitrogen an appropriate electrophile for the direct C–H amination. With these new insights, Leonori and co-workers developed a photocatalytic method to synthesize arylamines, using Ru(bipy)₃Cl₂ as photocatalyst.^{1,2} In this approach, a specific leaving group is installed either *ex situ*^{2,20} or *in situ*^{1,5} on the nitrogen atom of the coupling partner,

^aCentre for Membrane Separations, Adsorption, Catalysis and Spectroscopy for Sustainable Solutions (cMACS), KU Leuven, 3001 Leuven, Belgium.

E-mail: dirk.devos@kuleuven.be

^bKing Abdullah University of Science and Technology (KAUST), 23955 Thuwal, Saudi Arabia

†Electronic supplementary information (ESI) available: Detailed experimental procedures, optimization of the reaction conditions, kinetic experiments, additional characterization data and a thorough discussion on sustainability and economics. See DOI: <https://doi.org/10.1039/d3gc01225e>

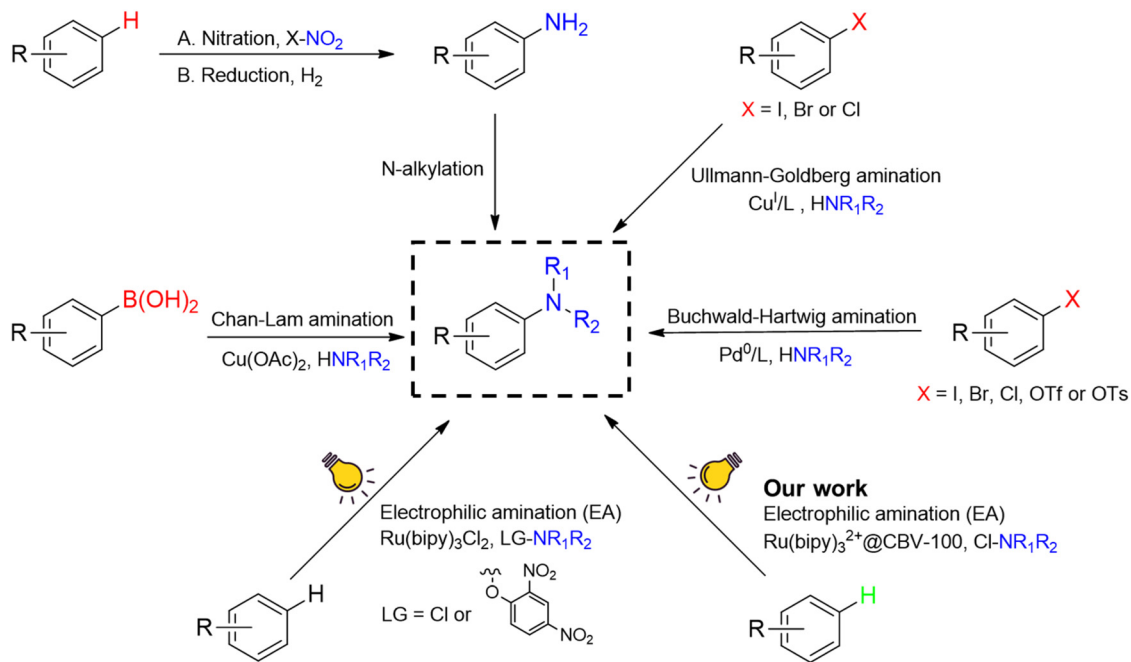


Fig. 1 Overview of the different approaches towards *N*-substituted arylamines.

which is transformed into a highly electrophilic aminium radical after a single electron transfer (SET) with the appropriate photocatalyst (Fig. 1).^{1,2,5,20,21}

Unfortunately, the homogeneous nature of these (photo) catalysts hampers their further adoption in large-scale processes due to the high cost and laborious post-synthetic removal of the catalyst from the reaction mixture. Therefore, heterogeneous catalysts are typically studied as promising and renewable alternatives, but they have rarely been considered for photocatalytic amination.^{22,23}

Faujasite type zeolites, which are aluminosilicates made up of SiO_4 and AlO_4 tetrahedra, are an appealing group of microporous, crystalline materials with a three-dimensional framework structure connected by interlinked voids.²⁴ These zeolite materials are currently applied in large-scale industrial processes (*e.g.* adsorption, FCC cracking,...) due to their low cost, high specific surface area (SSA), shape/size selectivity and high stability.²⁵ Besides the catalytic activity inherent to zeolites, the ability for metal cation exchange and for entrapment of (photoactive) organometallic complexes in their supercages are other important features allowing design of single-site heterogeneous catalysts.^{25,26–33}

In this work, a faujasite type zeolite Y material (CBV-100) is employed as host for the entrapment of $\text{Ru}(\text{bipy})_3^{2+}$ within its supercages *via* a “ship-in-a-bottle” technique (Fig. 1).²⁶ The entrapped photoactive polypyridyl complex can be excited by visible light to ultimately form electrophilic aminium radicals as the nitrogen coupling partner in direct C–H aminations. In this way, a single-site heterogeneous catalyst is developed for the sustainable synthesis of arylamines, while avoiding harsh conditions, stoichiometric amounts of transition metal and

pre-functionalized substrates (see ESI† for a detailed discussion on sustainability and economics).

Results and discussion

Synthesis and characterization of the catalyst

The faujasite CBV-100 [$[\text{Si}_{2.55}\text{Al}_{1.07.1}\text{Na}_1]$, with FAU topology and a silicon-to-aluminum ratio (SAR) of about 2.5 is commercially available; it is synthesized in aqueous media under hydrothermal conditions. This material is built up from sodalite cages, which are linked through double 6-membered rings (D6Rs).³⁴ In this way, the sodalite cages of faujasite are arranged in such a way that interconnected supercages are formed. This topology makes the material excellent as a support material to encapsulate $\text{Ru}(\text{bipy})_3^{2+}$ *via* a ship-in-a-bottle strategy.^{26,27} The zeolite material is first ion-exchanged with 1 wt% Ru using $\text{Ru}(\text{NH}_3)_6\text{Cl}_3$ in ultrapure demineralized water and subsequently contacted with an excess of molten 2,2'-bipyridine (bipy) to obtain the cationic photoactive complex (12 Å) in the 13 Å wide supercages.²⁷ The sample was excessively rinsed with acetone in order to remove excess ligand and complexes located on the outer surface. In order to determine the amount of entrapped photoactive molecules, the Ru-loaded zeolite was digested in aqua regia and HF; the Ru and the bipy were quantified by inductively coupled plasma atomic emission spectroscopy (ICP-OES) and ^1H nuclear magnetic resonance (NMR) of the liquid phase using added standards. The Ru content was estimated at 0.91 wt% (Table S1†), while the molar amount of coordinated bipy ligands was about 3× higher (Fig. S2 and S3†). Consequently,

12.9% of the supercages contained the Ru complex, leading to the single-site heterogeneous catalyst CBV-100-Ru(bipy)₃ [Si_{2.55}Al₁O_{7.1}Na_{0.956}(Ru(bipy)₃²⁺)_{0.022}]. Additionally, N₂ sorption analyses showed a significant decrease in micropore volume (45%) in comparison to the parent material (Fig. S4 and Table S2†).³⁵

The crystallinity and structure of the pristine and functionalized zeolite (CBV-100-Ru(bipy)₃) were confirmed by powder X-ray diffraction (PXRD) (Fig. 2A) and SEM (Fig. S5†). Furthermore, the location of the extra-framework cations is studied by the relative intensities of the XRD peaks with Miller indices 220, 331 and 311 (Fig. 2A). The cations are assumed to be randomly distributed within the lattice if $I_{331} > I_{220} > I_{311}$. However, upon impregnation of the zeolite with the photoactive complex, it is seen that $I_{331} > I_{311} > I_{220}$. We therefore presume that this is an indication that the formation of Ru(bipy)₃²⁺ in the supercages is accompanied by the displace-

ment of cations from their random positions in the supercages to locations inside the sodalite cages, at sites I' and II.^{36–38}

Additionally, spectroscopic techniques were employed in order to confirm the incorporation of the photoactive complex in the supercages of CBV-100. Fourier-transform infrared spectroscopy (FTIR) data confirm the presence of Ru(bipy)₃²⁺, since the characteristic bands in the region 1400 to 1500 cm⁻¹ resembles the C–N, C–C stretching vibrations and/or the C–H in-plane bending vibrations of the bipyridyl ligand (Fig. S6†).^{35,39} Furthermore, a typical absorption spectrum of Ru(bipy)₃Cl₂ in acetonitrile was collected, showing: (i) an intense band at 285 nm attributed to a π – π^* ligand-centered transition (LC), and (ii) a broad band from 380 nm to 500 nm in the visible region related to the metal-to-ligand charge transfer (MLCT) from the d-orbital of Ru to the π^* -orbital of the ligand (Fig. 2B).⁴⁰ A similar UV-Vis spectrum was measured for CBV-100-Ru(bipy)₃ in diffuse reflectance mode, with a

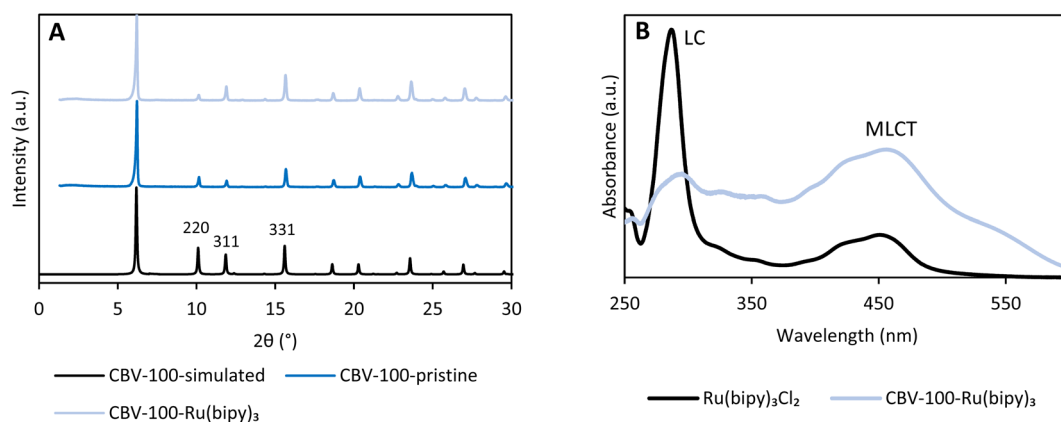


Fig. 2 XRD diffractogram of simulated CBV-100 (black), pristine CBV-100 (dark blue) and Ru loaded CBV-100-Ru(bipy)₃ (light blue) (A). UV-Vis spectrum of the homogeneous complex in acetonitrile (Ru(bipy)₃Cl₂, black) and a diffuse reflectance spectrum of CBV-100-Ru(bipy)₃ (blue) (B). LC = ligand centered transition, MLCT = metal-to-ligand charge transfer.

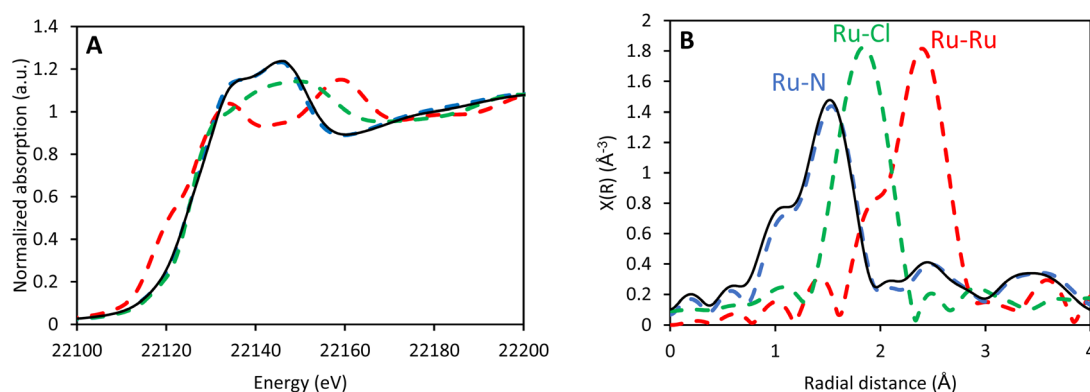


Fig. 3 XANES (A) and EXAFS (B) data for CBV-100-Ru(bipy)₃ (solid black) in comparison with reference samples (dashed lines): Ru(bipy)₃²⁺@EMC-1,²⁷ blue; RuCl₃, green; Ru-foil, red.

maximum at 456 nm, indicating that the photocatalyst can be excited in the visible-light region.

The oxidation state of the Ru center is of utmost importance, since only Ru(II) is susceptible to photoexcitation and can catalyze the amination reaction. X-ray absorption near-edge structure (XANES) of CBV-100-Ru(bipy)₃ confirms that the pattern is very similar to that previously recorded for Ru(bipy)₃²⁺@EMC-1 (EMC-1 is a faujasite with lowered Al-content; SAR = 3.6) (Fig. 3A).²⁷ Furthermore, the local environment of the encapsulated Ru center in the faujasite was studied by extended X-ray absorption fine structure (EXAFS) (Fig. 3B), which revealed that (i) the Ru-center is surrounded by six nitrogen atoms, (ii) no Ru-Cl interactions can be observed and (iii) the signals at higher radial distances (2–3 Å) can be assigned to the well-ordered carbon atoms of the 2,2'-bipyridine ligands. Moreover, the pattern and its intensity are similar to the pattern previously recorded for Ru(bipy)₃²⁺@EMC-1, which indicates that formation of the Ru-complex is successful. In addition, a good fit was obtained between the simulated spectrum of Ru(bipy)₃²⁺ and the measured spectrum of CBV-100-Ru(bipy)₃ (Fig. S7†).

Optimization of the reaction parameters

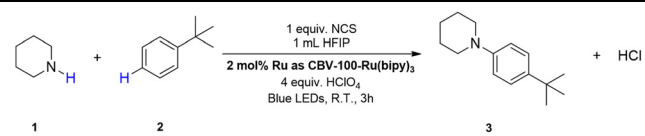
In order to check the performance of the heterogeneous single-site catalyst (*i.e.* CBV-100-Ru(bipy)₃) for the formation of

arylamines, piperidine and *t*-butylbenzene were employed as model substrates. *N*-Chlorosuccinimide (NCS) was first mixed together with the N-coupling partner in the solvent (HFIP). In this way, *N*-chloropiperidine was formed (Fig. S8†); next the solution was contacted with the strong acid (HClO₄) and the catalyst under the optimized reaction conditions (Table 1, entry 1).

Control experiments in the absence of NCS, light and catalyst were performed to verify the role of each compound in the product formation (Table 1, entries 3–5). The NCS reagent is essential for the chlorine transfer onto piperidine; in its absence, no electrophilic aminium radical and subsequently aminated arene can be formed (Table 1, entry 3).^{1,21,41} In the absence of light, no aminated arene product is observed, while the yield of chlorinated arene (70%) was extremely high (Table 1, entry 4). This suggests that the *N*-chloropiperidine displays an enhanced electrophilic character on the chlorine atom, which makes it an excellent reagent for the acid-catalyzed electrophilic aromatic chlorination (Fig. S9†).^{1,42,43} Furthermore, in the absence of catalyst, a product yield of 22% is observed due to the homolytic cleavage of the N–Cl bond.²¹ Additionally, the yield of chlorinated product is also high in this scenario (44%), which indicates the importance of the photocatalyst to kinetically overcome this dark background reaction.

A clear optimum is reached as the concentration of *t*-butylbenzene is varied in the reaction mixture (Fig. S10†). The yield of aminated arene remains moderate (30%) at low arene concentrations (2 equiv., Table 1, entry 6), while a remarkable increase in yield is noticed at higher concentrations. However, at an excessively large amount of the arene substrate the product yield remains unchanged (Table 1, entry 8). Furthermore, (in)organic acids with a low p*K*_a value (*i.e.* strong acids) are preferred, since protonation of *N*-chloropiperidine is more likely to occur (Fig. S11†).^{42–44} Nevertheless, a too strong acid (*e.g.* CF₃SO₃H, p*K*_a = –14.7) excessively stimulates the acid-catalyzed chlorination reaction and a decrease in C–N products is noticed. By varying the amount of acid (Table 1, entries 9–11), a similar effect was observed; the yield increases until the acid concentration becomes so high that it promotes the unwanted chlorination reaction (Fig. S12†).^{42,43} Generally, an increase of product yield is expected with a higher catalyst loading. However, at higher catalyst loadings, the yield remains unchanged (Table 1, entries 12, 13 and Fig. S13†). In order to understand this observation, the corresponding homogeneously catalyzed reactions were performed, with Ru(bipy)₃Cl₂ as catalyst; these clearly showed an increase of initial reaction rate and a lower amount of side products at higher catalyst loading (Fig. S14†). Such trend is not observed for the heterogeneously catalyzed reactions. This could be due to light penetration problems: because of too much diffuse scattering, the incoming light will not travel deeply into the reaction suspension at higher catalyst loading (*i.e.* when the suspension contains more zeolite material); therefore the volume fraction of the suspension that remains 'dark', and in which the chlorination dominates, is increased. In this way,

Table 1 Performance of the heterogeneous amination catalyst under different reaction conditions with piperidine and *t*-butylbenzene as model substrates



Entry	Conditions	Yield (Y ₃ ^b /Y ₄ ^c) (%)
1	Optimized conditions^a	64/19
2	Ru(bipy) ₃ Cl ₂ as catalyst	67/33
3	No NCS	0/0
4	No light	0/70
5	No catalyst	22/44
6	2 equiv. <i>t</i> -butylbenzene	30/6
7	8 equiv. <i>t</i> -butylbenzene	57/19
8	30 equiv. <i>t</i> -butylbenzene	62/16
9	0 equiv. HClO ₄	0/0
10	2 equiv. HClO ₄	19/19
11	16 equiv. HClO ₄	61/24
12	1 mol% Ru	49/15
13	5 mol% Ru	61/15
14	0.5 mmol piperidine	60/23
15	<i>N</i> -Hydroxypiperidine	0/0
16	Acetoxy- <i>N</i> -piperidine	0/0
17	Trifluoroacetoxy- <i>N</i> -piperidine	0/0

^a **1** (0.1 mmol), NCS (1 equiv.), 1 mL HFIP were mixed together and stirred for 30 minutes, afterwards **2** (18 equiv.), CBV-100-Ru(bipy)₃ (2 mol% Ru), HClO₄ (4 equiv.) were added and exposed to blue light (455–470 nm, 40 W) for 3 h at room temperature. ^b Y₃ is the yield of the arylamine **3**. ^c Y₄ is the summed yield of the chloro-*tert*-butylbenzenes.

the addition of more catalyst at a certain level no longer has an additional effect, and the correct amount of catalyst needs to be carefully considered. A kinetic study revealed that the initial reaction rate is significantly slower than for the corresponding homogeneously catalyzed reaction, which is easily explained by the hampered penetration of light into the zeolite crystals and by the diffusion limitations of substrate and product molecules through the zeolite framework (Fig. S15†).

Different leaving groups were installed on the piperidine molecule (*viz.* HO^- , $\text{CH}_3\text{C}(=\text{O})\text{O}^-$ and $\text{CF}_3\text{C}(=\text{O})\text{O}^-$) *via* a well-established pre-synthesis procedure.^{45,46} All these piperidine coupling partners were tested, but unfortunately

barely any yield is observed (Table 1, entries 15–17 and Fig. S16–S18†).

The support that was used for the synthesis of the heterogeneous single-site catalyst was the faujasite-type zeolite CBV-100. This zeolitic support is excellently suitable due to appropriate cage dimensions, which prevent the photoactive complex from leaching (Table S3†). By increasing the Si/Al ratio (SAR), a remarkable decline in product yield (Fig. 4) is observed due to a lower Ru-content in the zeolite framework after catalyst synthesis (Table S3†). Typically, these high SAR faujasites are produced from NaY *via* steaming processes, during which water steam is responsible for gradually etching away the aluminium from the framework, resulting in defects and mesopores.^{47,48} Therefore, some photocatalyst molecules are located in these mesopores with less pore size restriction, which results in Ru-leaching during the washing steps of the synthesis. On the other hand, high product yields were obtained with zeolite MCM-22 (MWW topology), even if its Ru-content is rather low (Table S3†). However, a large portion (~90%) of the Ru is leached during the reaction. This could be due to the fact that Ru here is located in the large half-cages located at the outer surface of the material (Table S4†). Even if a higher product yield of ~75% is obtained, the high activity is in fact due to the homogeneous nature of the catalyst during the reaction.

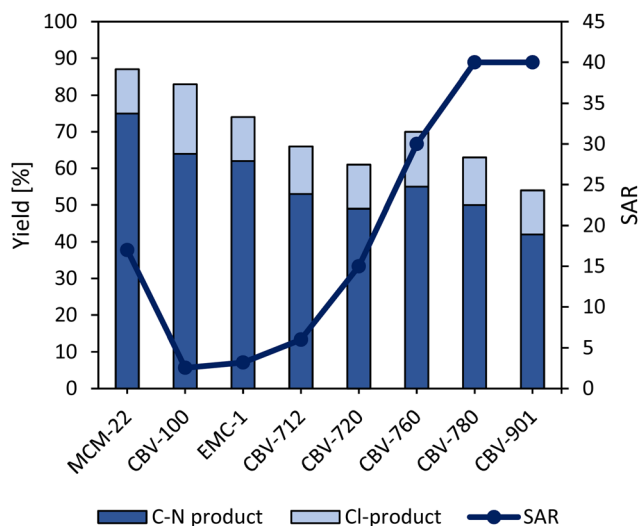


Fig. 4 Product yields (dark blue line) for $\text{Ru}(\text{bpy})_3^{2+}$ immobilized on zeolite supports with different SAR ratios (MCM-22 (SAR = 17), EMC-1 (SAR = 3.6), CBV-100 (SAR = 2.55), CBV-712 (SAR = 6), CBV-720 (SAR = 15), CBV-760 (SAR = 30), CBV-780 (SAR = 40) and CBV-901 (SAR = 40)). Reaction conditions: 0.1 mmol piperidine, 1 equiv. NCS, 18 equiv. *t*-butylbenzene, 4 equiv. HClO_4 , 1 mL HFIP, 2 mol% Ru as zeolite-Ru (theoretically), blue LEDs 3 h, R.T.

Strategies to overcome electrophilic chlorination: role of the solvent

Even if reaction conditions were thoroughly scrutinized, a significant amount of unwanted chlorinated products is still observed. To understand this better from a mechanistic point-of-view, we studied the homogeneous chlorination/amination of different arene substrates with *N*-chloropiperidine in more detail, using aromatics with weakly and increasingly strongly electron-donating substituents. The homogeneous photocatalyst $\text{Ru}(\text{bipy})_3\text{Cl}_2$ was used in either HFIP or acetonitrile (CH_3CN) (Fig. 5). Generally, a stronger electron donating effect

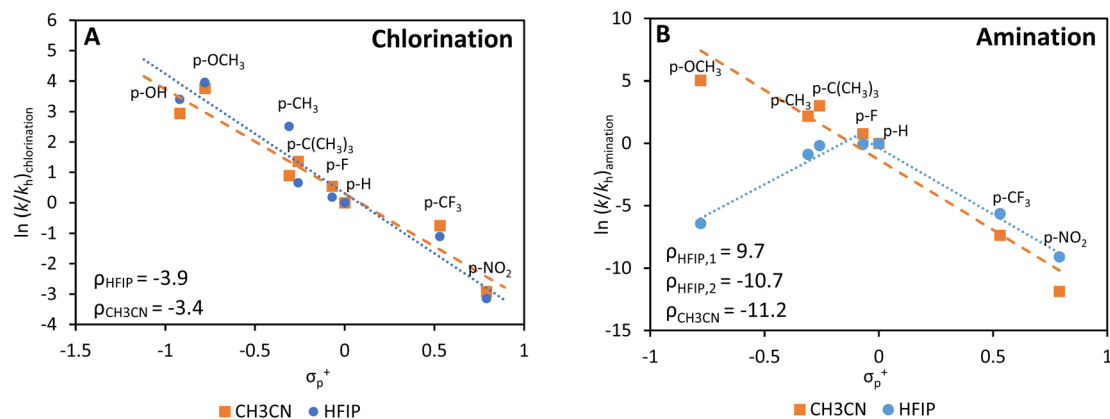


Fig. 5 Hammett plots of the homogeneous chlorination (A) and amination (B) reaction in HFIP and CH_3CN . Only the product with the Cl^- or amino-substituent on the *para* position is considered in these plots. Reaction conditions: 0.1 mmol piperidine, 1 equiv. NCS, 18 equiv. arene, 4 equiv. HClO_4 , 1 mL HFIP or CH_3CN , 2 mol% $\text{Ru}(\text{bipy})_3\text{Cl}_2$, 15 min, R.T.

of the substituent group results in a higher amount of chlorinated product, which is fully in line with the concept of electrophilic aromatic chlorination (Fig. 5A).^{49,50} While the trend is similar for both solvents, a slightly more negative ρ -value was noticed for HFIP, resulting in larger amounts of chlorinated arene as the substituent becomes more electron donating. The ability of HFIP to form H-bonds with the nitrogen atom of *N*-chloropiperidine may destabilize the N–Cl bond, which leads to the production of more chlorinated products if electron-rich arenes are available.^{51,52} Furthermore, the acidity of HFIP compared to that of CH₃CN may as well boost the acid catalyzed chlorination reaction.

On the other hand, a completely different trend is observed for the production of arylamines in HFIP and CH₃CN (Fig. 5B). The electrophilic nature of the aminium radical is readily confirmed by the monotonously linear plot in CH₃CN ($\rho = -11.2$); however, the Hammett plot obtained in HFIP displays a maximum, with lower rates for strongly electron-donating and electron-withdrawing groups. Surprisingly, by submitting the most electron-rich arenes to the reaction in HFIP, chlorination is preferred over amination due to the acidity and H-bond formation of this solvent (Fig. S19†).^{1,51,52} Overall, these experiments indicate that the preferred choice of the solvent is highly dictated by the electron density of the arene coupling partner: HFIP is suitable for electron-poor arenes, while CH₃CN is better used for electron-rich arenes.¹

Strategies to overcome electrophilic aromatic chlorination: role of temperature

The previous paragraph already revealed that the choice of a proper solvent for each arene molecule is important. However, the amount of chlorinated product is still considerable (Fig. 6) and therefore we considered the effect of

temperature on the heterogeneous reaction yield. As the temperature of the reaction mixture rises, the content of Cl-product increases and therefore, it seems more of interest to cool the reaction (Fig. S20†). *tert*-Butylbenzene, toluene and anisole are employed as coupling substrates in HFIP; the zeolite-based photocatalyst is used in conditions that are slightly adapted to minimize the amount of chlorination. By changing the solvent to CH₃CN for toluene and anisole, an increase in product yield was already observed, as explained in the previous paragraph (Fig. 6). By placing the samples in either an ice bath (0 °C) or an *o*-xylene/dry ice bath (−20 °C), the yield increases even further and the amount of chlorinated products becomes negligible (Fig. 6). Furthermore, upon cooling, the excited state of the photocatalyst is preserved longer, which could again favor the amination reaction.⁵³

Substrate scope

Aromatic coupling partners. With the optimized protocol for arene amination, we evaluated the arene scope using piperidine as our N-coupling partner (Fig. 7). The electrophilic nature of the aminium radical is clearly observed (3a–g), since the presence of strongly electron donating substituents can drastically improve the reaction yields. Furthermore, mono-substituted arenes provide mostly the *para*-products with high selectivity (3a, 3b, 3e–g); this phenomenon is also observed and explained by polar and steric effects in previous reports.^{1,2} *o*-, *m*- and *p*-xylene (3h–j) can be aminated in more drastic conditions (acetonitrile/dry ice bath (−40 °C)) to produce the corresponding arylamines in excellent to good yield (25–68%) with a single regio-isomer due to polar and steric effects of the methyl groups.^{1,2,54} Mesitylene (3k) on the other hand showed a very low yield towards the arylamine product, while an extremely large amount of chlorinated products is observed (97%).

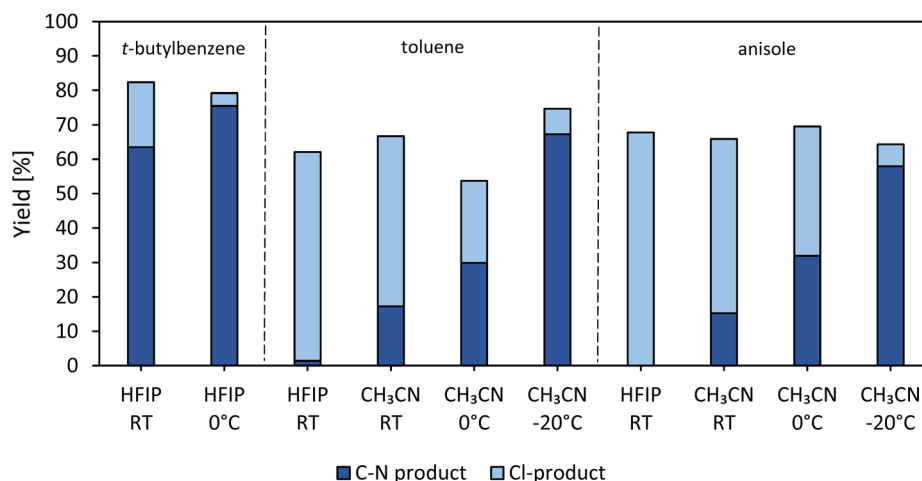
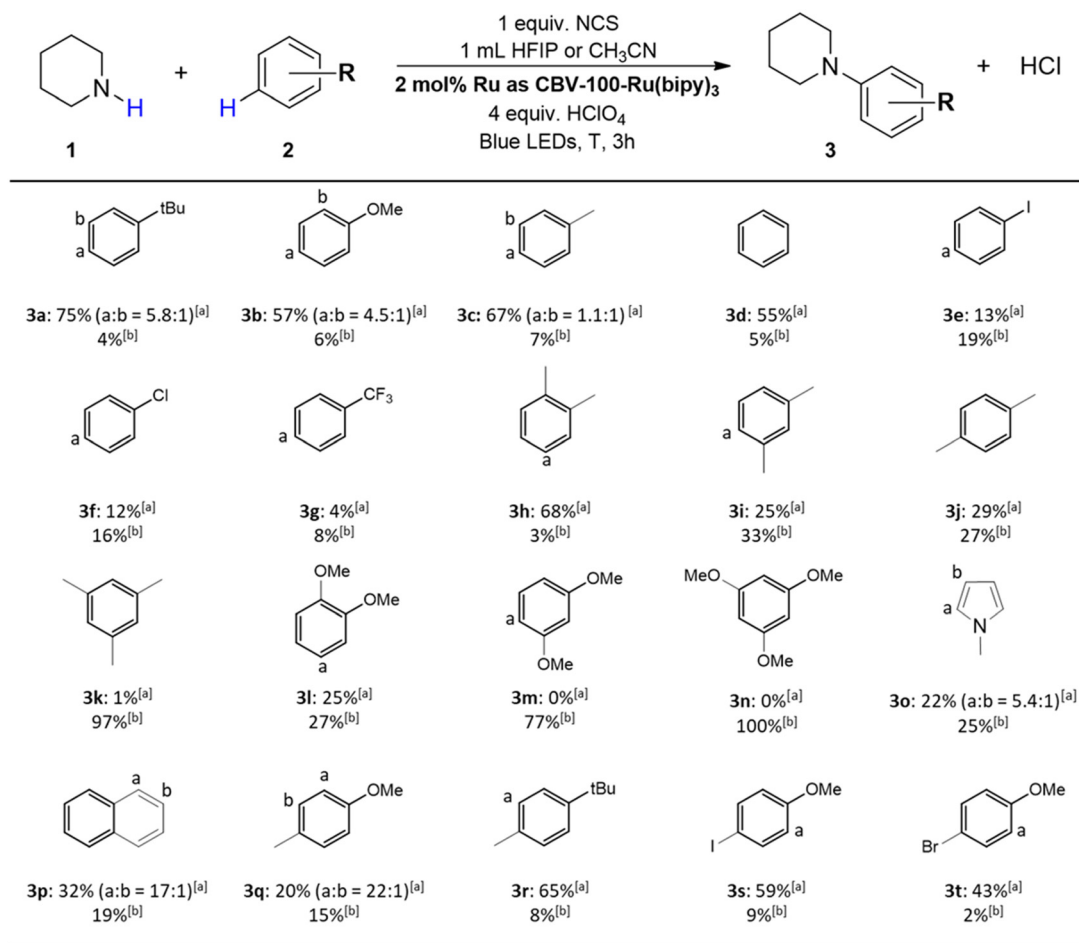


Fig. 6 Yields of heterogeneously catalyzed reactions with varying solvent and/or temperature (RT = room temperature, 0 °C and −20 °C). Reaction conditions: 0.1 mmol piperidine, 1 equiv. NCS, 18 equiv. arene, 4 equiv. HClO₄, 1 mL HFIP or CH₃CN, 2 mol% Ru as CBV-100-Ru(bipy)₃, blue LEDs, 3 h, R.T. Mixtures containing HFIP cannot be cooled until −20 °C.



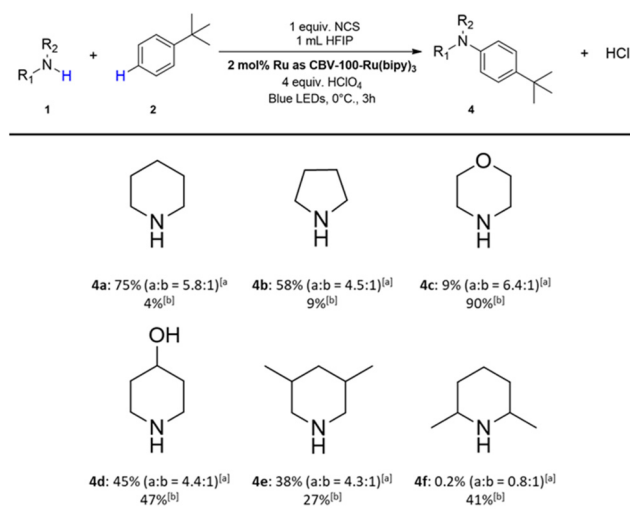
^[a]The yield of the arylamine products; the ratio of the products at the respective positions is given between brackets. ^[b]The yield of all chlorinated products (no distinction is made between the different types of chlorinated products).

Fig. 7 Substrate scope of different arene substrates. Reaction conditions: **1** (0.1 mmol), NCS (1 equiv.), 1 mL HFIP or CH₃CN were mixed together and stirred for 30 minutes, afterwards **2** (18 equiv.), CBV-100-Ru(bipy)₃ (2 mol% Ru), HClO₄ (4 equiv.) were added and the suspension was exposed to blue lights (455–470 nm, 40 W), for 3 h at 0 °C, –20 °C or –40 °C.

Even by using acetonitrile as solvent and upon strong cooling (–40 °C), no aminated product was detected due to (i) the steric hindrance exerted by the methyl substituents and (ii) the electron donating effect of the three methyl groups. A similar trend is also noticed when the methyl groups are replaced by methoxy groups (**3l–n**); 1,2-dimethoxybenzene gives the highest yield (25%), while 1,3-dimethoxy- and 1,3,5-trimethoxybenzene show barely any yield in combination with a strong formation of chlorinated products (77% and 100%, respectively). Moreover, halogenated anisoles (4-iodoanisole (**3s**) and 4-bromoanisole (**3t**)), which can be used as good precursors due to their halogen functionality, underwent amination in useful yields (59% and 43%).

Nitrogen coupling partners. Molecules containing piperidine rings are very prevalent in pharmaceutical industry, and typically substituent groups at the C3 and C4 positions of this heterocycle are regularly found.¹ With this in mind,

a scope of amine coupling partners was explored by applying *t*-butylbenzene as arene substrate (Fig. 8). Pyrrolidine (**4b**), which is another frequently used molecule in medicinal chemistry, is also well tolerated as coupling partner with a comparable yield as obtained with piperidine (58%). Additionally, the presence of oxygen in morpholine (**4c**) has a negative impact on the product yield (9%), since the rates of *N*-chloromorpholine and aminium radical formation are several orders slower due to its lower basicity ($pK_b = 5.6$).⁴¹ Furthermore, it is also noticed that the presence of substituent groups (like in **4d** and **4e**) does not affect the reactivity of the N-atom; therefore these substituents are well tolerated in the production of the corresponding arylamines. Nevertheless, the position of the substituent groups plays an important role, since undesirable steric effects could be observed, which results in low product yields (**4f**, 0.2%).



^[a]The yield of the arylamine products, the ratio of the products at the respective positions is given between brackets. ^[b]The yield of all chlorinated products (no distinction is made between the different types of chlorinated products).

Fig. 8 Substrate scope of different N-coupling partners. Reaction conditions: 1 (0.1 mmol), NCS (1 equiv.), 1 mL HFIP were mixed together and stirred for 30 minutes, afterwards 2 (18 equiv.), CBV-100-Ru(bipy)₃ (2 mol% Ru), HClO₄ (4 equiv.) were added and the suspension was placed under blue lights (455–470 nm, 40 W), for 3 h at 0 °C.

Heterogeneity and recyclability of the catalyst

A recyclability test is executed to verify the heterogeneous nature of the catalyst. This test demonstrates a small decline in product yield after four recycling runs (Fig. 9A). ICP-OES analysis demonstrates that over 99% of the catalyst's activity is retained since the total amount of Ru-leach-

ing in the reaction solvent is estimated at <1%, which is probably attributed to the fine fraction of the zeolite powder (Table S5†). Furthermore, the PXRD diffractogram at the end of the four consecutive runs shows an identical pattern as the pristine CBV-100 material; and no significant loss in long-range order is observed (Fig. S21†). Moreover, the filtrate collected after 30 min during a so-called filtration test (Fig. 9B) shows only a small increase in product yield after 3 h due to the homolytic, light induced cleavage of the N–Cl bond (Table 1, entry 4).

Conclusion

In this work, we reported a direct coupling of amine compounds and aromatics under photoredox conditions. The photoactive complex Ru(bipy)₃²⁺ is synthesized within the supercages of a faujasite type zeolite (*i.e.* CBV-100) and its entrapment was successfully verified by PXRD, N₂-physisorption, FTIR, UV-Vis and XAS. CBV-100 was selected as the ideal support, since leaching during catalyst synthesis and/or amination reaction was not observed. Furthermore, the direct C–H amination reaction was studied in detail using Hammett plots, and the proper reaction conditions for each arene substrate were selected, with acetonitrile being preferred for electron-rich arenes and HFIP for electron-poor arenes. Knowing these optimal conditions, the arene and amine substrate scope were explored to indicate the suitability of the heterogeneous catalyst in this coupling reaction. Finally, the heterogeneity of the catalyst was confirmed *via* recycling/filtration tests and metal analysis of the reaction mixture indicated that Ru-leaching was very limited. These results provide new insight into the development of heterogeneous zeolite-based photocatalysts, since Ru(bipy)₃²⁺ is commonly used in photocatalytic applications.

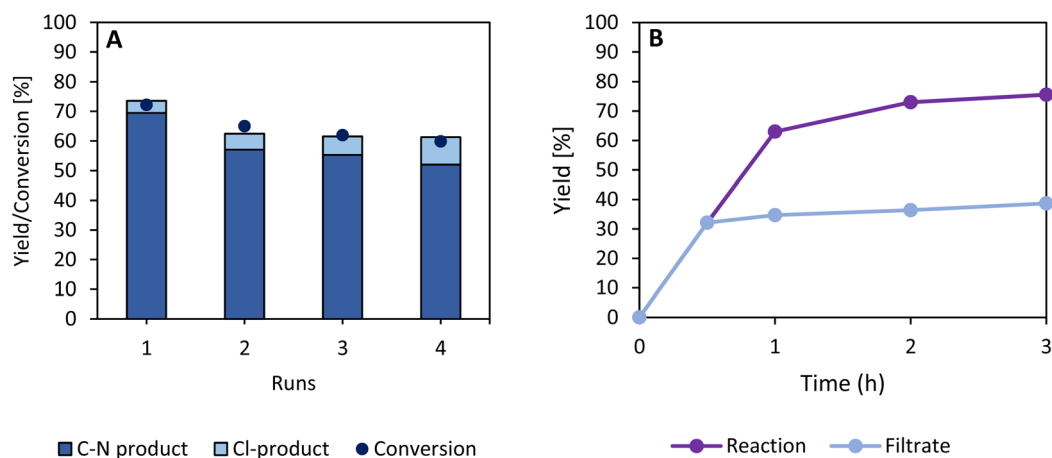


Fig. 9 Recyclability test for four consecutive runs. A small reduction in yield was observed after four runs (A). After the reaction, the mixture was centrifuged, the reaction solution was removed and the zeolite was washed with ultrapure water and dried. Subsequently, fresh reaction mixture was added to the zeolite and a second/third/fourth run was executed. Filtration test was performed and filtrate was collected after 30 minutes to check the heterogeneity of the reaction (B).

Conflicts of interest

The Authors declare no conflict of interest.

Acknowledgements

The research leading to these results has received funding from the KAUST-CRG Program (OSR-2018-CRG7-3741.2). K. J. and D. E. D. V. thank FWO for project funding (grant no. G0F2320N). We acknowledge the SUPERXAS beamline at Swiss Light source (SLS, Switzerland) for providing the beamtime and Dr. Aram Bugaev for the professional support during the measurements. V. L. is thanking Carlos Marquez for the ICP-OES measurements.

References

- 1 A. Ruffoni, F. Julia, T. D. Svejstrup, A. J. McMillan, J. J. Douglas and D. Leonori, *Nat. Chem.*, 2019, **11**(5), 426–433.
- 2 T. D. Svejstrup, A. Ruffoni, F. Julia, V. M. Aubert and D. A. Leonori, *Angew. Chem., Int. Ed.*, 2017, **56**(47), 14948–14952.
- 3 L. Van Emelen, M. Henrion, R. Lemmens and D. De Vos, *Catal. Sci. Technol.*, 2022, **12**(2), 360–389.
- 4 P. Patnaik, *A comprehensive guide to the hazardous properties of chemical substances*, 2007, pp. 251–268.
- 5 S. C. Cosgrove, J. M. C. Plane and S. P. Marsden, *Chem. Sci.*, 2018, **9**(32), 6647–6652.
- 6 S. L. Rössler, B. J. Jeliet and P. F. Tripet, *Angew. Chem., Int. Ed.*, 2019, **58**(2), 526–531.
- 7 F. Ullmann, *Ber. Dtsch. Chem. Ges.*, 1903, **36**(2), 2382–2384.
- 8 C. Sambigao, S. P. Marsden, A. J. Blacker and P. C. McGowan, *Chem. Soc. Rev.*, 2014, **43**(10), 3525–3550.
- 9 I. Goldberg, *Ber. Dtsch. Chem. Ges.*, 1906, **39**, 5–6.
- 10 F. Benaskar, V. Engels, E. V. Rebrov, N. G. Patil, J. Meuldijk, P. C. Thüne, P. C. M. M. Magusin, B. Mezari, V. Hessel, L. A. Hulshof, E. J. M. Hensen, A. E. H. Wheatley and J. C. Schouten, *Chem. – Eur. J.*, 2012, **18**, 1800–1810.
- 11 K. Mullick, S. Biswas, C. Kim, R. Ramprasad, A. M. Angeles-Boza and S. L. Suib, *Inorg. Chem.*, 2017, **56**, 10290–10297.
- 12 W. Long, W. Qiu, C. Guo, C. Li, L. Song, G. Bai, G. Zhang and H. He, *Molecules*, 2015, **20**, 21178–21192.
- 13 D. Berthold, A. M. Haydl, J. C. Leung, U. Scholz, Q. Xiao and Z. Zhu, *Methodol. Amine Synth.*, 2021, **10**, 377–444.
- 14 D. M. T. Chan, K. L. Monaco, R. P. Wang and M. P. Winters, *Tetrahedron Lett.*, 1998, **39**(19), 2933–2936.
- 15 P. Y. S. Lam, C. G. Clark and S. Saubern, *Tetrahedron Lett.*, 1998, **39**(19), 2941–2944.
- 16 M. J. West, J. W. B. Fyfe, J. C. Vantourout and A. J. B. Watson, *Chem. Rev.*, 2019, **119**(24), 12491–12523.
- 17 D. S. Surry and S. L. Buchwald, *Angew. Chem., Int. Ed.*, 2008, **47**(34), 6338–6361.
- 18 J. F. Hartwig, *Acc. Chem. Res.*, 2008, **41**(11), 1534–1544.
- 19 H. Kim and S. Chang, *ACS Catal.*, 2016, **6**(4), 2341–2351.
- 20 L. J. Allen, P. J. Carbrera, M. Lee and M. S. Sanford, *J. Am. Chem. Soc.*, 2014, **136**(15), 5607–5610.
- 21 J. M. Ganley, P. R. D. Murray and R. R. Knowles, *ACS Catal.*, 2022, **10**(20), 11712–11738.
- 22 M. Xu, Y. Hua, X. Fu and J. Liu, *Chem. – Eur. J.*, 2022, **28**(15), e202104394.
- 23 Y. Y. Liu, D. Liang, L. Q. Lu and W. J. Xiao, *Chem. Commun.*, 2019, **55**(33), 4853–4856.
- 24 R. Broach, D. Y. Jan and D. Lesch, *Ullmann's Encyclopedia of Industrial Chemistry*, 2012.
- 25 A. Corma and H. Garcia, *Chem. Commun.*, 2004, 1443–1459.
- 26 W. DeWilde, G. Peeters and J. H. Lunsford, *J. Phys. Chem.*, 1980, 2306–2310.
- 27 V. Lemmens, C. Vos, A. L. Bugaev and D. De Vos, *ACS Appl. Mater. Interfaces*, 2022, **14**(1), 971–977.
- 28 N. Taira, M. Saitoh, S. Hashimoto, H. R. Moon and K. B. Yoon, *Photochem. Photobiol. Sci.*, 2006, **5**(9), 822–827.
- 29 Y. S. Park, E. J. Lee, Y. S. Chun, Y. D. Yoon and K. B. Yoon, *J. Am. Chem. Soc.*, 2002, **124**(24), 7123–7135.
- 30 F. Binder, G. Calzaferri and N. Gfeller, *Sol. Energy Mater. Sol. Cells*, 1995, **38**(1–4), 175–186.
- 31 M. Sykora, K. Maruszewski, S. M. Treffert-Ziemelis and J. R. Kincaid, *J. Am. Chem. Soc.*, 1998, **120**(14), 3490–3498.
- 32 A. Moissette, M. Hureau, P. Col and H. Venzin, *Microporous Mesoporous Mater.*, 2017, **254**, 128–135.
- 33 H. Garcia and H. D. Roth, *Chem. Rev.*, 2002, **102**(11), 3947–4007.
- 34 D. Martinez and J. Perez-Pariente, *Zeolites and Ordered Porous Solids: Fundamentals and Applications*, 2011.
- 35 S. Komaty, H. Özçelik, M. Zaarour, A. Ferre, S. Valable and S. Mintova, *J. Colloid Interface Sci.*, 2021, **581**, 919–927.
- 36 W. H. Quayle and J. H. Lunsford, *Inorg. Chem.*, 1982, **21**(1), 97–103.
- 37 M. Nakayama, J. Yano, K. Nakoaka and K. Ogura, *Synth. Met.*, 2003, **138**(3), 419–422.
- 38 A. Kozlov, K. Asakura and Y. Iwasawa, *Microporous Mesoporous Mater.*, 1998, **21**(4–6), 571–579.
- 39 M. U. Munshi, J. Martens, G. Berden and J. Oomens, *J. Phys. Chem. A*, 2020, **124**(12), 2449–1459.
- 40 K. Mori, M. Kawashima, K. Kagohara and H. Yamashita, *J. Phys. Chem. C*, 2008, **112**(49), 19449–19455.
- 41 C. Pastoriza, J. M. Antelo, J. Crujeiras and A. Pena-Gallego, *J. Phys. Org. Chem.*, 2014, **27**(5), 407–418.
- 42 J. R. L. Smith, L. C. McKeer and J. M. Taylor, *J. Chem. Soc., Perkin Trans. 2*, 1989, 1529–1536.
- 43 S. J. Lee, M. S. Terraza, D. J. Pippel and P. Beak, *J. Am. Chem. Soc.*, 2003, **125**, 7307–7312.
- 44 F. Minisci, *Synthesis*, 1973, 1–24.
- 45 Z. Zhang, Y. Yu and L. S. Liebeskind, *Org. Lett.*, 2007, **10**(14), 3005–3008.

- 46 J. K. Kerkovius and F. A. Menard, *Synthesis*, 2016, **48**(11), 1622–1629.
- 47 W. Lutz, C. H. Rüschler and T. M. Gesing, *Stud. Surf. Sci. Catal.*, 2004, **154**, 1411–1417.
- 48 R. A. Beyerlein, C. Choi-feng, J. B. Hall, B. J. Huggins and G. J. Ray, *Top. Catal.*, 1997, **4**(1–2), 27–42.
- 49 B. Ellis and R. Smith, *Polymers: A Property Database*, 2nd edn, 2000.
- 50 H. C. Brown and Y. Okamoto, *J. Am. Chem. Soc.*, 1957, **79**(8), 1913–1917.
- 51 I. Colomer, A. E. R. Chamberlain, M. B. Haughey and T. J. Donohoe, *Nat. Rev. Chem.*, 2017, **1**(11), 0088.
- 52 R. J. Tang, T. Milcent and B. Crousse, *J. Org. Chem.*, 2018, **83**(2), 930–938.
- 53 M. K. Brennaman, J. H. Alstrum-Acevedo, C. N. Fleming, P. Jang, T. J. Meyer and J. M. Papanikolas, *J. Am. Chem. Soc.*, 2002, **124**(50), 15094–15098.
- 54 R. J. Tang, P. Retailleau, T. Milcent and B. Crousse, *ACS Omega*, 2019, **4**(5), 8690–8966.